

2-2-2024

## Thermo-hydro-mechanical coupling model for natural gas hydrate-bearing sediments with depressurization based on OpenGeoSys

Zhi-gang YE

*Key Laboratory of Soft Soils and Geoenvironmental Engineering of the Ministry of Education, Zhejiang University, Hangzhou, Zhejiang 310058, China; Institute of Geotechnical Engineering, Zhejiang University, Hangzhou, Zhejiang 310058, China; Center for Hypergravity Experimental and Interdisciplinary Research, Zhejiang University, Hangzhou, Zhejiang 310058, China, zhigangye@zju.edu.cn*

Lu-jun WANG

*Key Laboratory of Soft Soils and Geoenvironmental Engineering of the Ministry of Education, Zhejiang University, Hangzhou, Zhejiang 310058, China; Institute of Geotechnical Engineering, Zhejiang University, Hangzhou, Zhejiang 310058, China; Center for Hypergravity Experimental and Interdisciplinary Research, Zhejiang University, Hangzhou, Zhejiang 310058, China, lujunwang@zju.edu.cn*

Bin ZHU

*Key Laboratory of Soft Soils and Geoenvironmental Engineering of the Ministry of Education, Zhejiang University, Hangzhou, Zhejiang 310058, China; Institute of Geotechnical Engineering, Zhejiang University, Hangzhou, Zhejiang 310058, China; Center for Hypergravity Experimental and Interdisciplinary Research, Zhejiang University, Hangzhou, Zhejiang 310058, China*

Yun-min CHEN

*Key Laboratory of Soft Soils and Geoenvironmental Engineering of the Ministry of Education, Zhejiang University, Hangzhou, Zhejiang 310058, China; Institute of Geotechnical Engineering, Zhejiang University, Hangzhou, Zhejiang 310058, China; Center for Hypergravity Experimental and Interdisciplinary Research, Zhejiang University, Hangzhou, Zhejiang 310058, China*

### Recommended Citation

YE, Zhi-gang; WANG, Lu-jun; ZHU, Bin; and CHEN, Yun-min (2024) "Thermo-hydro-mechanical coupling model for natural gas hydrate-bearing sediments with depressurization based on OpenGeoSys," *Rock and Soil Mechanics*: Vol. 44: Iss. 11, Article 5.

DOI: 10.16285/j.rsm.2023.6012

Available at: <https://rocksoilmch.researchcommons.org/journal/vol44/iss11/5>

---

# Thermo-hydro-mechanical coupling model for natural gas hydrate-bearing sediments with depressurization based on OpenGeoSys

## Abstract

Natural gas hydrates are considered as one of the most important potential alternatives for energy shortage, and depressurization is believed to be the most economic effectiveness for hydrate exploitation. The exploitation induces solid hydrate dissociation, liquid / gas generation and migration, heat transfer and skeleton deformation, showing strong thermo-hydro-mechanical (THM) coupling behavior of sediments. These processes will trigger geotechnical hazards, such as borehole inclination and reservoir collapse. A THM coupling numerical model for hydrate exploitation was developed based on the open-source FEM platform OpenGeoSys. In detail, the kinetic reaction equation was implemented to represent the liquid/gas generation during gas hydrate dissociation. Air and water mass balance equations were introduced to illustrate the phase change between liquid and gas phases. Besides, the nonlinear complementarity problem (NCP) combined with the choice of special primary variables was adopted to strictly constrain the liquid / gas saturation, and kinetic reaction rate was connected to the source/sink terms of governing equations. The model was validated and verified through a test and a large-scale numerical model, and the effects of pore water compressibility on the THM coupling response of hydrate-bearing sediments were discussed. Results show that the model was numerically stable in dealing with the nonlinear problems of phase change among solid, liquid and gas phases, and of phase appearance / disappearance of pore fluids caused by hydrate dissociation; the hydrates dissociate from near to far regions, and the produced gas / liquid gradually migrated to the driving well and reached a steady state, where the gas / liquid saturation tended to be stable; due to the influence of air dissolution, the evolution of gas phase saturation lagged behind that of the liquid saturation; the pore water compressibility had a non-negligible effect on the dissipation of pore pressure and skeleton deformation under large pore pressure.

## Keywords

hydrate-bearing sediments, depressurization, numerical model, thermo-hydro-mechanical coupling, OpenGeoSys

# Thermo-hydro-mechanical coupling model for natural gas hydrate-bearing sediments with depressurization based on OpenGeoSys

YE Zhi-gang<sup>1,2,3</sup>, WANG Lu-jun<sup>1,2,3</sup>, ZHU Bin<sup>1,2,3</sup>, CHEN Yun-min<sup>1,2,3</sup>

1. Key Laboratory of Soft Soils and Geoenvironmental Engineering of the Ministry of Education, Zhejiang University, Hangzhou, Zhejiang 310058, China

2. Institute of Geotechnical Engineering, Zhejiang University, Hangzhou, Zhejiang 310058, China

3. Center for Hypergravity Experimental and Interdisciplinary Research, Zhejiang University, Hangzhou, Zhejiang 310058, China

**Abstract:** Natural gas hydrates are considered as one of the most important potential alternatives for energy shortage, and depressurization is believed to be the most economic effectiveness for hydrate exploitation. The exploitation induces solid hydrate dissociation, liquid / gas generation and migration, heat transfer and skeleton deformation, showing strong thermo-hydro-mechanical (THM) coupling behavior of sediments. These processes will trigger geotechnical hazards, such as borehole inclination and reservoir collapse. A THM coupling numerical model for hydrate exploitation was developed based on the open-source FEM platform OpenGeoSys. In detail, the kinetic reaction equation was implemented to represent the liquid/gas generation during gas hydrate dissociation. Air and water mass balance equations were introduced to illustrate the phase change between liquid and gas phases. Besides, the nonlinear complementarity problem (NCP) combined with the choice of special primary variables was adopted to strictly constrain the liquid / gas saturation, and kinetic reaction rate was connected to the source/sink terms of governing equations. The model was validated and verified through a test and a large-scale numerical model, and the effects of pore water compressibility on the THM coupling response of hydrate-bearing sediments were discussed. Results show that the model was numerically stable in dealing with the nonlinear problems of phase change among solid, liquid and gas phases, and of phase appearance / disappearance of pore fluids caused by hydrate dissociation; the hydrates dissociate from near to far regions, and the produced gas / liquid gradually migrated to the driving well and reached a steady state, where the gas / liquid saturation tended to be stable; due to the influence of air dissolution, the evolution of gas phase saturation lagged behind that of the liquid saturation; the pore water compressibility had a non-negligible effect on the dissipation of pore pressure and skeleton deformation under large pore pressure.

**Keywords:** hydrate-bearing sediments; depressurization; numerical model; thermo-hydro-mechanical coupling; OpenGeoSys

## 1 Introduction

Natural gas hydrates are cage-like crystalline compounds formed by gas molecules (e.g. methane and ethane) and water molecules at high pressures and low temperatures which are widely distributed in marine sediments<sup>[1]</sup>. It has been estimated that the carbon equivalent of hydrate reservoirs is at least twice as much as that of conventional fossil energy sources<sup>[2–3]</sup>. The decomposition of hydrate during production can absorb a large amount of heat from the surrounding geotechnical environment and weaken the stiffness and strength of the soil aggregate<sup>[4–7]</sup>. The gas and water generated by the hydrate decomposition can change the pore pressure and affect the effective stress of the soil aggregate and the convective heat transfer of the fluids. In addition, the change of temperature causes the thermal expansion of the solid-liquid-gas phases and the change of the decomposition rate, and the deformation of the soil aggregate can also affect the accumulation and dissipation of the pore pressure in turn. The hydrate production processes involve strong thermo-hydro-mechanical (T-H-M) coupling between the above phases. The long-term hydrate production process may lead to obvious changes in the

effective stress of the reservoir and uneven spatial distribution, which may induce catastrophes such as tilting of the production wells and collapse of the reservoir seafloor<sup>[8–10]</sup>. Therefore, it is essential to study the T-H-M coupling of sediment in the hydrate production process to ensure safe and efficient production.

Currently, in situ production test of gas hydrates has been conducted in several countries, including Russia<sup>[11]</sup>, Canada<sup>[12]</sup>, the United States<sup>[13]</sup>, Japan<sup>[14–15]</sup>, and China<sup>[16–17]</sup>. In the 1960s, the world's first hydrate production test using the depressurization method was conducted in the Messoyakha oilfield in Russia<sup>[11]</sup>. In 2002, 2007 and 2008, Canada conducted the in situ hydrate production tests using the depressurization method in the Mackenzie Delta of the Northwest Territories<sup>[12]</sup>. In 2012, the Ignik Sikumi field trial on the North Slope of Alaska, USA, was designed to explore the potential value of the CO<sub>2</sub>-CH<sub>4</sub> exchange method for commercial hydrate extraction<sup>[13]</sup>. In 2013 and 2017, Japan conducted the production test of marine gas hydrates in the Nankai Trough using the depressurization method<sup>[14–15]</sup>, and the 1st and 2nd trial AT1-P3 wells were terminated due to sanding. In 2017 and 2020, China conducted the production test

Received: 12 July 2023

Accepted: 11 September 2023

This work was supported by the Fundamental Research Funds for the Central Universities (226-2023-00083) and National Natural Science Foundation (51988101, 52078458).

First author: YE Zhi-gang, male, born in 1992, PhD, research interests: multiphase and multi-field interactions in marine geotechnical engineering. E-mail: zhigangye@zju.edu.cn

Corresponding author: WANG Lu-jun, male, born in 1985, PhD, Associate Professor, research interests: mechanical properties of hydrate-bearing sediments and multiphase and multi field coupling of soil. E-mail: lujunwang@zju.edu.cn

using the depressurization method in the Shenhu Sea area of the South China Sea<sup>[16–17]</sup>, and the average daily gas production rates were  $0.51 \times 10^4$  and  $2.87 \times 10^4$  m<sup>3</sup>, respectively. These field test mines are of significant value, but for commercial extraction, the rate of gas production from marine sediments tends to be up to  $5.0 \times 10^5$  m<sup>3</sup>/d<sup>[18–19]</sup>. According to this value, there is still a large gap between the most sites of hydrate field production test and the commercial production.

Due to the high cost and long period of in situ production test, numerical simulation has become an effective method to study the response characteristics of hydrate production reservoirs. Many researchers in the world have carried out relevant numerical studies on the coupled T-H-M response of sediments caused by hydrate production by adopting different software, including Tough+Hydrate+Flac/Biot<sup>[20–21]</sup>, Comsol<sup>[22–23]</sup>, Code-Bright<sup>[24]</sup> and QIMGHyd-THMC<sup>[25]</sup>. Wilder et al.<sup>[26]</sup> and White et al.<sup>[27]</sup> summarized the functions and features of different multi-field coupled numerical software and methods for hydrate decomposition production. Rutqvist et al.<sup>[20]</sup> used Tough+Hydrate+Flac method to simulate the hydrate decompression production process in two permafrost layers and found that the hydrate decomposition caused an increase in shear stress in the decomposition region, which was detrimental to the stability of the production wells. Sun et al.<sup>[22]</sup> introduced the thermodynamic-based constitutive relations in Comsol to study the static and dynamic characteristics of sediments during hydrate decomposition. Sánchez et al.<sup>[24]</sup> simulated the gas production characteristics and freezing phenomena during hydrate decomposition using Code-Bright. The above work investigated the physicochemical properties of hydrate sediments and the multi-field responses in the production process from various perspectives.

Marine hydrate deposits are generally located at water depths of kilometers and hundreds of meters below the seabed, with pore pressures of tens of MPa. It has been shown that the depressurization is the most economically feasible and efficient production method<sup>[14,28]</sup>, and the pressure drop is transmitted rapidly in the process of hydrate production using depressurization, while the expended pore water caused by the pressure drop will rapidly replenish the pore space, which leads to the difference in the pressure drop amplitude at different distances, and thus has a different impact on the deformation of the skeleton. In addition, the hydrate sediments are often initially saturated with water, and the conventional non-isothermal multiphase flow theory has difficulty in rigorously describing the processes such as gas dissolution caused by the hydrate decomposition, which gradually reaches the maximum solubility and precipitates the free gas, as well as in simulating the special conditions such as saturation at the bottom of the hydrate layer and unsaturation at the top of the hydrate layer under the action of gravity<sup>[29–30]</sup>. This phase transition process is one of the most important processes in the study of

two-phase flow, where the pore fluid may be in a single-phase or two-phase state depending on the conditions of pressure, temperature and phase composition, and this phase transition produces discontinuities in the primary or secondary variables such as saturation. To address this issue, researchers have proposed different numerical methods. The first method is to change the combination of the primary variables according to the current phase state, also known as primary variable switching (PVS)<sup>[31–32]</sup>. The second type is a two-phase approach for flash calculation, known as phase stability analysis and phase separation<sup>[33–34]</sup>. The third type is the persistent primary variable (PPV) method<sup>[35]</sup>, which employs non-standard primary variables such as generalized mass density or extends the definition of variables such as saturation or capillary pressure to take into account processes such as phase transition<sup>[36–37]</sup>. However, the above methods have some limitations. For instance, the frequent switching of the PVS principal variables may introduce numerical oscillations in the Newtonian iteration, leading to non-convergence. For flash calculation method, the minimum Gibbs free energy calculations in the phase stability analysis usually lead to high computational costs. The PPV suffers from numerical difficulties in describing the disappearance of the liquid phase<sup>[37]</sup>. In view of such problems, Lauser et al.<sup>[38]</sup> introduced a new method to formulate the process of phase disappearance or emergence as a nonlinear complementarity problem (NCP), which can effectively solve the above difficulties.

Considering the above processes and the current status of numerical software for hydrate multi-field coupling that are mostly commercial (e.g. Tough+Hydrate+Flac and Comsol) or free of charge but difficult to modify the source code (e.g. Code-Bright and QIMGHyd-THMC). This paper introduces the NCP combined with special primary variable selection to develop a coupled T-H-M analytical model for natural gas hydrate extraction, based on the open-source multi-phase multi-field coupling finite element software OpenGeoSys. The correctness of the developed model is verified by comparing the laboratory decomposition test and the large-scale numerical model of hydrate production using depressurization method. The validity of the analytical model NCP was verified by combining with the simulation of the gas phase generation process of the large-scale model, and the validity of the liquid-gas saturation was determined by strictly selecting the special primary variables. In addition, the effect of pore water compressibility on the T-H-M coupling process in the extraction process is numerically analyzed, and the numerical stability of the model in dealing with the solid-liquid-gas phase transition caused by solid-phase hydrate decomposition and the pore fluid phase generation/disappearance and other extremely nonlinear problems is discussed. A new open-source finite element model is provided for the analytical simulation of T-H-M coupling in natural gas hydrate production using depressurization

method.

## 2 Theory of thermo-hydraulic coupling for hydrate-bearing sediments

### 2.1 Governing equations

The above T-H-M coupling in the production process of hydrate-bearing sediments includes the processes of solid-liquid-gas phase transition, pore water and gas transport, heat transfer and skeleton deformation. The following basic assumptions are introduced: (1) the soil skeleton and pore water are in thermal balance; (2) the heat conduction and heat convection are considered for heat transfer; (3) the Darcy's law and the Fick's law are adopted to describe the liquid-gas seepage and diffusion processes, and the phase transition between liquid water and water vapor is considered; and (4) the hydrate phase transition due to kinetic decomposition is considered, but the secondary generation of hydrate is not taken into account. Based on the above assumptions, the following governing equations for mass conservation, energy conservation and conservation of linear momentum are established with the primary variables including pore water pressure  $p_L$ , total molar fraction of gas components  $X^a$ , temperature  $T$  and displacement  $u$ .

#### 2.1.1 Mass conservation equations

The mass conservation equations for pore water and gas can be expressed separately as follows:

$$\left. \begin{aligned} & \frac{d_s}{dt} (N_L \varphi_L x_L^w + N_G \varphi_G x_G^w) + \\ & \nabla (N_L x_L^w \mathbf{q}_L + N_L \mathbf{J}_L^w + N_G x_G^w \mathbf{q}_G + N_G \mathbf{J}_G^w) + \\ & (N_L \varphi_L x_L^w + N_G \varphi_G x_G^w) \nabla \frac{d_s \mathbf{u}}{dt} = q_w \\ & \frac{d_s}{dt} (N_L \varphi_L x_L^a + N_G \varphi_G x_G^a) + \\ & \nabla (N_L x_L^a \mathbf{q}_L + N_L \mathbf{J}_L^a + N_G x_G^a \mathbf{q}_G + N_G \mathbf{J}_G^a) + \\ & (N_L \varphi_L x_L^a + N_G \varphi_G x_G^a) \nabla \frac{d_s \mathbf{u}}{dt} = q_a \end{aligned} \right\} \quad (1)$$

where  $d_s$  is the material derivative based on the solid phase;  $t$  is the time;  $N_L$  and  $N_G$  are the molar densities of the liquid and gas phases;  $\varphi_L$  and  $\varphi_G$  are the volume fractions of the liquid and gas phases;  $x_L^w$  and  $x_G^w$  are the molar fractions of the liquid water and water vapor;  $x_L^a$  and  $x_G^a$  are the molar fractions of the dissolved gas and the dry gas;  $q_w$  and  $q_a$  are the source/sink terms of the water and gas produced by the hydrate phase transition;  $\mathbf{q}_L$  and  $\mathbf{q}_G$  are the relative flow velocities of the liquid and gas phases (Eq. (2));  $\mathbf{J}_L^w$  and  $\mathbf{J}_G^w$  are the diffusion fluxes of the liquid water and the water vapor; and  $\mathbf{J}_L^a$  and  $\mathbf{J}_G^a$  are the diffusion fluxes of the dissolved gas and the gaseous gas.

$$\left. \begin{aligned} \mathbf{q}_L &= -\frac{\mathbf{K}_p k_{relL}}{\mu_L} (\nabla p_L - \rho_L \mathbf{g}) \\ \mathbf{q}_G &= -\frac{\mathbf{K}_p k_{relG}}{\mu_G} (\nabla p_G - \rho_G \mathbf{g}) \end{aligned} \right\} \quad (2)$$

where  $\mathbf{K}_p$  is the intrinsic permeability;  $p_G$  is the pore gas pressure;  $k_{relL}$  and  $k_{relG}$  are the relative permeability coefficients for the liquid and gas phases;  $\mu_L$  and  $\mu_G$  are the viscosity coefficients for the liquid and gas phases; and  $\mathbf{g}$  is the gravitational constant vector.

$$\left. \begin{aligned} \mathbf{J}_L^w &= -\frac{\varphi_L}{\tau_L} \mathbf{D}_L^w \nabla x_L^w \\ \mathbf{J}_G^w &= -\frac{\varphi_G}{\tau_G} \mathbf{D}_G^w \nabla x_G^w \\ \mathbf{J}_L^a &= -\frac{\varphi_L}{\tau_L} \mathbf{D}_L^a \nabla x_L^a \\ \mathbf{J}_G^a &= -\frac{\varphi_G}{\tau_G} \mathbf{D}_G^a \nabla x_G^a \end{aligned} \right\} \quad (3)$$

where  $\tau_L$  and  $\tau_G$  are the liquid and gas phase tortuosities;  $\mathbf{D}_L^w$  and  $\mathbf{D}_L^a$  are the diffusion tensors for liquid water and dissolved gas; and  $\mathbf{D}_G^w$  and  $\mathbf{D}_G^a$  are the diffusion tensors for water vapor and dry gas.

#### 2.1.2 Energy conservation equations

The heat conduction and convective heat transfer due to pore water and gas transport, as well as the gas phase volume efforts, are considered in the heat transfer process:

$$\frac{d_s}{dt} (u_L \varphi_L \rho_L + u_G \varphi_G \rho_G + u_H \varphi_H \rho_H + u_s \varphi_s \rho_s) + \nabla (\mathbf{J}_c + h_L \rho_L \mathbf{q}_L + h_G \rho_G \mathbf{q}_G) = q_E \quad (4)$$

where  $\mathbf{J}_c$  is the heat transfer flux;  $\rho_L$ ,  $\rho_G$ ,  $\rho_H$ , and  $\rho_s$  are the densities of the liquid phase, gas phase, hydrate, and solid phase;  $u_L$ ,  $u_G$ ,  $u_H$ , and  $u_s$  are the specific energies of the liquid phase, gas phase, hydrate, and solid phase;  $h_L$  and  $h_G$  are the specific enthalpies of the liquid and gas phases; and  $q_E$  is the energy source/sink term from the hydrate phase transition.

The relationship between the specific energy and specific enthalpy of the gas can be expressed as follows:

$$\left. \begin{aligned} u_G &= h_G - \frac{p_G}{\rho_G} \\ h_G &= x_G^a h_G^a \frac{M_a}{M_G} + x_G^w h_G^w \frac{M_w}{M_G} \\ h_G^a &= \int_{T_0}^T C^a dT + \frac{RT}{M_a} \\ h_G^w &= \int_{T_0}^T C^w dT + h_{\Delta E} \end{aligned} \right\} \quad (5)$$

where  $h_G^a$  and  $h_G^w$  are the specific enthalpies of gas phase dry gas and gas phase water vapor;  $M_G$  is the molar mass of the gas phase mixture;  $h_{\Delta E}$  is the enthalpy change of evaporation of liquid water into water vapor;  $C^a$  and  $C^w$  are the specific heat capacities of gas and water;  $T_0$  is the initial temperature;  $M_a$  is the molar mass of gas;  $M_w$  is the molar mass of water; and  $R$  is the ideal gas constant.

2.1.3 Equation of conservation of linear momentum

The equation of conservation of linear momentum can be expressed as follows after ignoring the effects of the inertial force and the velocity gradient of the pore fluid:

$$\nabla \sigma + (\rho_s(1-\varphi) + \rho_H s_H \varphi + \rho_L s_L \varphi + \rho_G s_G \varphi) \mathbf{g} = 0 \quad (6)$$

where  $\sigma$  is the total stress; and  $\varphi$  is the porosity. The total stress  $\sigma$  is related to the effective stress  $\sigma'$  as follows:

$$\left. \begin{aligned} \sigma &= \sigma' - p_L \frac{s_L}{1-s_H} \mathbf{l} - p_G \frac{s_G}{1-s_H} \mathbf{l} \\ \sigma' &= \mathbf{D}^e : (\boldsymbol{\varepsilon} - \boldsymbol{\varepsilon}_T) = \mathbf{D}^e : \frac{\nabla \mathbf{u} + \nabla^T \mathbf{u}}{2} - \mathbf{D}^e : \alpha^T (T - T_0) \end{aligned} \right\} \quad (7)$$

where  $s_L$ ,  $s_G$ , and  $s_H$  are the saturations for the liquid phase, gas phase, and hydrate; the superscript T is the transposed symbol;  $\mathbf{l}$  is the unit tensor;  $\mathbf{D}^e$  is the linear elasticity tensor, which can be determined according to the Young's modulus and Poisson's ratio;  $\boldsymbol{\varepsilon}$  is the total strain tensor;  $\boldsymbol{\varepsilon}_T$  is the thermal strain tensor; and  $\alpha^T$  is the coefficient of thermal expansion of the solid phase.

2.2 Nonlinear complementarity problems for liquid-gas phase transition

The liquid-gas phase transition is a crucial process in non-isothermal two-phase flow and often causes discontinuities for the primary or secondary variables or strong nonlinearities in the energy conservation equations. Frequent switching of the primary variables in the PVS may introduce numerical oscillations in Newtonian iterations, and there are numerical difficulties in solving for the disappearance of liquid phase in PPV. Lauser et al.<sup>[38]</sup> introduced a new approach to formulate the process of phase disappearance or generation as the NCP. The NCP method constructs a set of non-differentials but semi-smooth equations that can be solved by the semi-smooth Newton-Raphson method<sup>[39]</sup>. The main advantage of the NCP method is the use of a fixed set of primary variables and a system of nonlinear equations, which avoids switching of the primary variables. Another advantage is that the phase stability analyses are not required due to the presence of complementarity conditions. In this paper, the NCP method was introduced to address the multi-field coupling problem of hydrate phase transition in order to describe the non-isothermal two-phase flow process.

Hence, the local constraint equations can be constructed as follows:

$$\left. \begin{aligned} \min [s_L, 1 - (x_L^w + x_L^a)] &= 0 \\ \min [s_G, 1 - (x_G^w + x_G^a)] &= 0 \\ X^a - \frac{N_L \varphi_L x_L^a + N_G \varphi_G x_G^a}{N_L \varphi_L + N_G \varphi_G} &= 0 \end{aligned} \right\} \quad (8)$$

The above partial constraint equation can be written as follows:

$$\left. \begin{aligned} f_{\text{constr1}} &= \min [s_L, 1 - (x_L^w + x_L^a)] \\ f_{\text{constr2}} &= \min [s_G, 1 - (x_G^w + x_G^a)] \\ f_{\text{constr3}} &= N_L s_L (X^a - x_L^a) + N_G s_G (X^a - x_G^a) \end{aligned} \right\} \quad (9)$$

The above system of partial equations can be denoted as  $\mathbf{F}$ . Using the Newton-Raphson iterative method to solve it, the Jacobian matrices of  $\mathbf{F}$  for the partial principal state variable  $\mathbf{X}_{\text{local}}$  and the global principal variable  $\mathbf{X}$  are given by the following equations:

$$\left. \begin{aligned} \frac{\partial \mathbf{F}}{\partial \mathbf{X}_{\text{local}}} &= \begin{Bmatrix} \frac{\partial f_{\text{constr1}}}{\partial s_L} & \frac{\partial f_{\text{constr1}}}{\partial x_L^w} & \frac{\partial f_{\text{constr1}}}{\partial x_G^a} \\ \frac{\partial f_{\text{constr2}}}{\partial s_L} & \frac{\partial f_{\text{constr2}}}{\partial x_L^w} & \frac{\partial f_{\text{constr2}}}{\partial x_G^a} \\ \frac{\partial f_{\text{constr3}}}{\partial s_L} & \frac{\partial f_{\text{constr3}}}{\partial x_L^w} & \frac{\partial f_{\text{constr3}}}{\partial x_G^a} \end{Bmatrix} \\ \frac{\partial \mathbf{F}}{\partial \mathbf{X}} &= \begin{Bmatrix} \frac{\partial f_{\text{constr1}}}{\partial p_L} & \frac{\partial f_{\text{constr1}}}{\partial X^a} & \frac{\partial f_{\text{constr1}}}{\partial T} \\ \frac{\partial f_{\text{constr2}}}{\partial p_L} & \frac{\partial f_{\text{constr2}}}{\partial X^a} & \frac{\partial f_{\text{constr2}}}{\partial T} \\ \frac{\partial f_{\text{constr3}}}{\partial p_L} & \frac{\partial f_{\text{constr3}}}{\partial X^a} & \frac{\partial f_{\text{constr3}}}{\partial T} \end{Bmatrix} \end{aligned} \right\} \quad (10)$$

Then the relationship between  $\mathbf{X}_{\text{local}}$  and  $\mathbf{X}$  can be expressed as follows:

$$\frac{\partial \mathbf{X}_{\text{local}}}{\partial \mathbf{X}} = \left( \frac{\partial \mathbf{F}}{\partial \mathbf{X}_{\text{local}}} \right)^{-1} \frac{\partial \mathbf{F}}{\partial \mathbf{X}} \quad (11)$$

Therefore, the relationship between  $\mathbf{X}_{\text{local}}$  and  $\mathbf{X}$  is established, i.e. the current state variables such as partial liquid-gas saturation can be determined according to  $\mathbf{X}$ , and then the partial liquid-gas two-phase state can be related to the overall governing equations.

2.3 Liquid-gas two-phase state equations

The gas phase consists of water vapor and dry gas, with the partial pressure of water vapor  $p_G^w$  following the Raoult's law and the solubility of the gas component following the Henry's law:

$$\left. \begin{aligned} \frac{x_G^w}{x_L^w} &= \frac{p_G^w}{p_G} \\ \frac{x_L^a}{x_G^a} &= \frac{H^a p_G}{N_L} \end{aligned} \right\} \quad (12)$$

where  $H^a$  is Henry constant.  $p_G^w$  and saturated vapor pressure  $p_{\text{satG}}^w$  are determined by the Kelvin-Laplace and Clausius-Clapeyron equations:

$$\left. \begin{aligned} p_G^w &= p_{\text{satG}}^w \exp \left( -\frac{p_C}{N_L RT} \right) \\ p_{\text{satG}}^w &= p_{\text{satG0}}^w \exp \left( \left( \frac{1}{T} - \frac{1}{T_0} \right) \frac{h_{\Delta E} M_w}{R} \right) \end{aligned} \right\} \quad (13)$$

where  $p_c$  is the capillary pressure; and  $p_{\text{satG}0}^w$  is the saturated vapor pressure corresponding to a temperature of  $T_0$ .

The relationship between  $p_c$  and  $s_L$  is described by the soil-water retention curve (SWRC), which can be modeled using various approaches such as the Brooks-Corey model and the van Genuchten model. When the effect of  $s_H$  is taken into account, it can be expressed uniformly as follows:

$$p_c = p_c(s_L, s_H) \quad (14)$$

The relative permeability coefficients of liquid-gas phase are also related to their respective saturations and can be affected by  $s_H$ . The classical models, such as the Brooks-Corey model, the van Genuchten model and the Corey model, can be uniformly expressed as follows:

$$\left. \begin{aligned} k_{\text{relL}} &= k_{\text{relL}}(s_L, s_H) \\ k_{\text{relG}} &= k_{\text{relG}}(s_G, s_H) \end{aligned} \right\} \quad (15)$$

### 2.4 Phase transition equations of hydrate kinetic decomposition

During the hydrate decomposition process, the solid phase hydrate decomposes and transitions to water and gas, which changes the properties of the solid phase skeleton. Meanwhile, a large amount of heat is absorbed during the hydrate decomposition. Currently, there are several models to quantitatively describe the hydrate decomposition process, such as the equilibrium model, the anthropomorphic chemical kinetic model, and the chemical kinetic model.

The Kim-Bishnoi kinetic model is the most widely used model currently, which is adopted in this paper. This model considers that the actual reaction rate is determined by the activation energy and specific surface area, which can be expressed as follows:

$$\left. \begin{aligned} R_r &= K_d A_s (p_E - p_G) \\ K_d &= K_0 \exp\left(-\frac{\Delta E}{RT}\right) \end{aligned} \right\} \quad (16)$$

where  $R_r$  is the decomposition rate;  $K_d$  is the kinetic decomposition rate;  $K_0$  is kinetic decomposition constant;  $\Delta E$  is the activation energy; and  $A_s$  is the decomposition specific surface area, which is related to the porosity and hydrate saturation, and  $A_s = \varphi s_H A_{s0}$ ,  $A_{s0} = 7.5 \times 10^5 \text{ 1/m}^{[22]}$ ; and  $p_E$  is the phase equilibrium pressure, which can be expressed as follows:

$$p_E = \exp\left(a + \frac{b}{T}\right) \quad (17)$$

where  $a$  and  $b$  are balance pressure parameters of hydrate phase.

Based on this, the mass rate and energy rate for the aforementioned water and gas are available as follows:

$$\left. \begin{aligned} q_w &= N_H M_w R_r \\ q_a &= M_a R_r \\ q_E &= -\Delta H M_H R_r \end{aligned} \right\} \quad (18)$$

where  $N_H$  is the hydrate stoichiometric number, representing the ratio of the number of moles of water to that of gas during the hydrate decomposition; and  $\Delta H$  is the enthalpy change, which is usually related to the temperature:

$$\Delta H = C_0 + C_1 T \quad (19)$$

where  $C_0$  and  $C_1$  are parameters related to the hydrate enthalpy change.

Based on this, the liquid-gas mass and energy rates due to hydrate decomposition can be solved quantitatively based on  $X$  with the liquid-gas two-phase state determined by the NCP, and the correlation can be established with the governing equations through the source/sink term.

## 3 Multi-field coupled analysis model

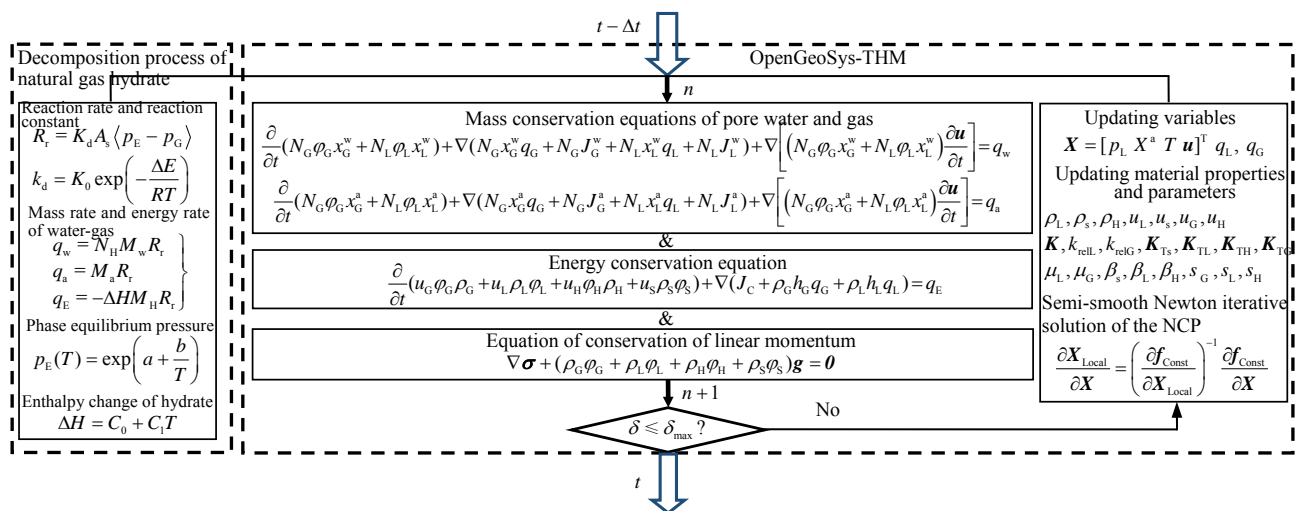
### 3.1 Modeling and solving

OpenGeoSys is an open-source finite element numerical platform developed for the study of multiphase multi-field interaction in porous media. It consists of various functional models to study the coupling problems of different fields through the development and invocation of different models. OpenGeoSys is highly expandable and can be modified according to the demand of the governing equations or the development of a specific solution model. The nonlinear iteration is performed using either the Newton-Raphson method or the Picard method, while the linear iteration is performed using the mature open-source solver Eigen database or the built-in BiCGSTAB, CG, and SparseLU methods in the PETSc database, which provide good numerical computational stability and high efficiency.

As shown in Fig. 1, this paper developed a coupled T-H-M analysis model for hydrate production based on the existing saturated soil T-H-M model in the OpenGeoSys platform. The saturated soil T-H-M model contains the equations of pore water mass conservation, energy conservation and conservation of linear momentum. The pore water transport follows the Darcy's law. The heat transfer consists of heat conduction and thermal convection due to pore water transport. The soil skeleton follows the linear theory of elasticity and the Terzaghi's effective stress principle. On the global level, the analytical model in this paper needs to additionally introduce the mass conservation equation of pore gas, in order to establish the governing equations for the mass conservation, energy conservation and conservation of linear momentum of the pore water and gas. This is different from the conventional method of using  $X = [p_L / p_c \ p_G \ T \ u]^T$  as the primary variable<sup>[22, 40]</sup>. The primary variable of this model was chosen as  $X = [p_L \ X^a \ T \ u]^T$  to unify the description of the single-phase state saturated with water and the gas-liquid two-phase state, i.e. from the initial saturated liquid phase to the gradual precipitation of free gas,  $p_c$  did not change, and the conventional primary variables  $p_L / p_c$  and  $p_G$  were difficult to describe the process, but in this

model,  $X^a$  can be changed while maintaining  $p_C$  constant. Different from saturated soil, the pore water and gas transport in this model can be extended to include convection and diffusion, following the Darcy's law and the Fick's law. The heat convection induced by pore gas was considered for heat transfer, and the effective stresses were considered for both  $p_L / p_C$  and  $p_G$ , employing the Bishop's principle of effective stress, which simultaneously considered the effects of liquid phase, gas phase, and hydrate saturation. On the local level, the NCP constraint equations were embedded for the liquid-gas phase state solution, and the physical range of liquid-gas saturation was strictly limited. At this time, it was necessary to introduce the state equations such as the Clausius-Clapeyron ideal gas equation, the Raoult's law, the Henry's law, the Kelvin-Laplace water vapor pressure equation, and the relative permeability function, to establish the relationships between gas phase density and pressure, water vapor molar fraction and liquid water molar fraction, dry gas molar fraction and dissolved gas molar fraction, saturated vapor pressure and temperature/capillary pressure, and liquid-gas permeability and saturation. Meanwhile, the kinetic decomposition process of hydrate phase transition after decomposition was solved at the local level, including the equations of Kim-Bishnoi reaction rate, reaction constant, specific surface area of reaction, phase equilibrium pressure and enthalpy change. The reaction rate was related to the source/sink terms of the mass and energy equations to determine the processes of water production, gas production and heat absorption caused by the hydrate phase transition after

decomposition. The saturation, density, specific heat capacity, intrinsic permeability, relative permeability coefficient, heat conduction and thermal expansion coefficient were then updated. Combining the above processes with appropriate pre-processing (e.g. Gmsh) and post-processing (e.g. Paraview) software, a model can be built to solve the above governing equations (Eqs. (1), (4), and (6)). In this model, the full coupling between the governing equations was adopted to improve the solution accuracy, the Newton-Raphson method was used for the nonlinear iteration, and the BICGSTAB method was used for the linear iteration. In the hydrate production process, the solid phase hydrate decomposition, gas and liquid production, liquid phase evaporation and condensation, and gas phase dissolution and desolvation have strong nonlinearities, which are easy to cause numerical oscillations and instability of the solution. In this paper, the NCP in the model strictly restricted the gas-liquid saturation range from the mathematical-physical level to ensure the local mass conservation, which is advantageous for addressing this type of strong nonlinear problem. In addition, the selection of the global primary variable  $X$  and the construction of the local NCP in the model can effectively and uniformly describe the single-phase and two-phase flow states, as well as the liquid-gas interconversion process between both. Therefore, the model in this paper has better solution stability and accuracy in addressing strong nonlinear problems caused by solid-liquid-gas and liquid-gas phase transitions, and can further realize the division of larger time steps on this basis to achieve higher solution efficiency.



Note:  $K_{Ts}$ ,  $K_{TL}$ ,  $K_{TH}$ , and  $K_{TG}$  are the thermal conductivity tensors of solid phase, liquid phase, gas phase, and hydrate;  $\beta_s$ ,  $\beta_L$ , and  $\beta_H$  are the thermal expansion coefficients of the volume of the solid phase, liquid phase, and hydrate;  $\Delta t$  is the time increment;  $\delta$  and  $\delta_{max}$  are the current iterative step error and the allowable iterative error; and  $n$  is the number of local iterative steps.

Fig. 1 Diagram of THM coupling model induced by natural gas hydrate production

### 3.2 Model validation

#### 3.2.1 Validation of laboratory test of hydrate decomposition using depressurization method

In order to verify the accuracy of the coupled T-H-M analytical model presented in this paper, the

corresponding numerical model was established and compared with the test of hydrate decomposition using depressurization conducted by Masuda et al.<sup>[41]</sup>. The model geometry, mesh division, boundary conditions, and the temperature measurement points, P1 to P3, are

shown in Fig. 2.

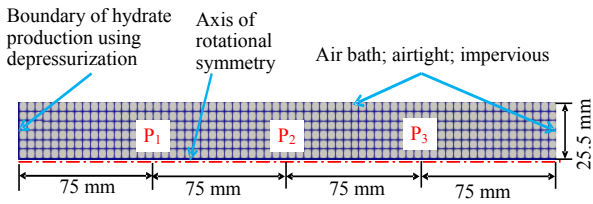


**Fig. 2 Mesh division and boundary conditions of Masuda's test**

The initial temperature of the model was 275.45 K, the initial pressure was 3.75 MPa, the production boundary pressure was 2.84 MPa, the porosity was 0.182, the initial saturations of the liquid phase, gas phase and hydrate were 0.443, 0.206 and 0.351, and the Young's modulus and Poisson's ratio of the hydrate sediment were 300 MPa and 0.35. The Brooks-Corey model was adopted to describe the soil-water characteristic curve, and the Corey model was used to reproduce the liquid-gas relative permeability. The intrinsic permeability was found to be affected by hydrate saturation<sup>[22, 40]</sup>, and the enthalpy change was related to the temperature. The detailed expressions and their parameters and the parameters including density, specific heat capacity and heat transfer coefficient of each phase of soil, water, gas and hydrate are shown in Tables 1 and 2.

As shown in Figs. 3(a), 3(b) and 3(c), the results of the present model, such as temperature and air pressure versus gas production, were relatively consistent with the experiments<sup>[41]</sup> and the available numerical results<sup>[22, 40]</sup>. It can be noted that there were some discrepancies between the measured data<sup>[41]</sup> and the numerical results in terms of temperature and gas pressure. The

temperature was overestimated by the present model simulation in the time period from 0 to 6 000 s, which may be caused by the Joule-Thomson effect<sup>[42]</sup>, i.e. the gas absorbs more heat when it is released from the hydrate. For the gas pressure, neither Sun et al.<sup>[22]</sup> nor the results of the present model fully reflected the local peak around 3 000 s. Deng et al.<sup>[42]</sup> suggested that this peak may be due to the Joule-Thomson effect resulting from the compression coefficient of the gas phase and the specific surface area related to the intrinsic permeability. Although the temperature of P3 in the simulation of Sun et al.<sup>[22]</sup> was more accurate, the simulation aspects of the model presented in this paper for gas pressure and gas production matched the measured values better. In the model of Sun et al.<sup>[22]</sup>, gas diffusion and water vapor flux were not considered, whereas the model in this paper considered the effects of these factors. Comparing with the numerical simulation of Ye et al.<sup>[40]</sup>, the results showed a better agreement. The difference between the two models is that the present model was based on the NCP to construct the solution to the local non-isothermal two-phase flow equation of state, while Ye et al.<sup>[40]</sup> was based on the solution to the conventional non-isothermal two-phase flow equation of state, and there were also differences between the two models in the selection of the primary variables. The advantage of this model is that it is stable and efficient in addressing strong nonlinear problems such as solid-liquid-gas phase transition and phase generation/disappearance through the introduction of NCP. In addition, it can be easily developed and extended to solve more complex, large-scale hydrate extraction problems in the field.

**Table 1 Primary parameters of the model and their values<sup>[22, 41]</sup>**

Model parameter	Expression	Value
SWRC	$p_c = p_0 (s_E)^{1/n_{pc}}; s_E = \frac{s_L / (1 - s_H) - s_{Gr} - s_{Lr}}{1 - s_{Gr} - s_{Lr}}$	$p_0 = 1\ 000\ \text{kPa}; n_{pc} = 0.65; s_{Gr} = 0; s_{Lr} = 0.1$
Relative permeability coefficient	$k_{relL} = \left( \frac{s_L - s_{Lr}}{1 - s_{Lr}} \right)^{n_L}; k_{relG} = \left( \frac{s_G - s_{Gr}}{1 - s_{Gr}} \right)^{n_G}$	$n_L = 3.0; n_G = 3.0$
Intrinsic permeability /m <sup>2</sup>	$K = \begin{cases} K_0 \left( \frac{\varphi}{\varphi_0} \right)^{\frac{3}{2}} \left( \frac{1 - \varphi}{1 - \varphi_0} \right)^3 (1 - s_{H0})^{N_p} & s_H > s_{Hc} \\ K_0 \left( \frac{\varphi}{\varphi_0} \right)^{\frac{3}{2}} \left( \frac{1 - \varphi}{1 - \varphi_0} \right)^3 \left( 1 - \frac{s_H}{s_{Hc}} (1 - (1 - s_{H0})^{N_p}) \right) & s_H < s_{Hc} \end{cases}$	$K_0 = 9.67 \times 10^{-4}; \varphi_0 = 0.182; N_p = 5.2; s_{Hc} = 0.000\ 1$
Enthalpy change /( $\text{J} \cdot \text{mol}^{-1}$ )	$\Delta H = C_0 + C_1 T$	$C_0 = 55\ 380.44; C_1 = -16.47$

Note:  $p_0$  is the intake suction value;  $s_E$  is the effective saturation;  $s_{Gr}$  and  $s_{Lr}$  are the residual saturations of the gas and liquid phases, respectively;  $n_{pc}$ ,  $n_L$  and  $n_G$  are the correlation coefficients of the pore distribution;  $K_0$  is the initial intrinsic permeability;  $\varphi_0$  is the initial porosity;  $s_{Hc}$  is the critical hydrate saturation;  $s_{H0}$  is the initial hydrate saturation; and  $N_p$  is the correlation coefficient of the intrinsic permeability.

**Table 2 Parameters of different phases<sup>[22, 41]</sup>**

Parameter	Density /( $\text{kg} \cdot \text{m}^{-3}$ )	Specific heat capacity /( $\text{J} \cdot \text{kg}^{-1} \cdot \text{K}^{-1}$ )	Thermal conductivity coefficient /( $\text{W} \cdot \text{m}^{-1} \cdot \text{K}^{-1}$ )	Viscosity coefficient /( $\text{Pa} \cdot \text{s}$ )	Coefficient of thermal expansion /( $\text{m} \cdot \text{K}^{-1}$ )	Molar mass /( $\text{kg} \cdot \text{mol}^{-1}$ )
Soil	2 600	800	8.800 0	—	$1.5 \times 10^{-5}$	—
Hydrate	910	2 000	0.393 0	—	$1.5 \times 10^{-5}$	0.124
Liquid phase	1 000	4 200	0.556 0	$1 \times 10^{-3}$	$4.0 \times 10^{-4}$	0.018
Gas phase	—	2 100	0.033 5	$7 \times 10^{-6}$	—	0.016

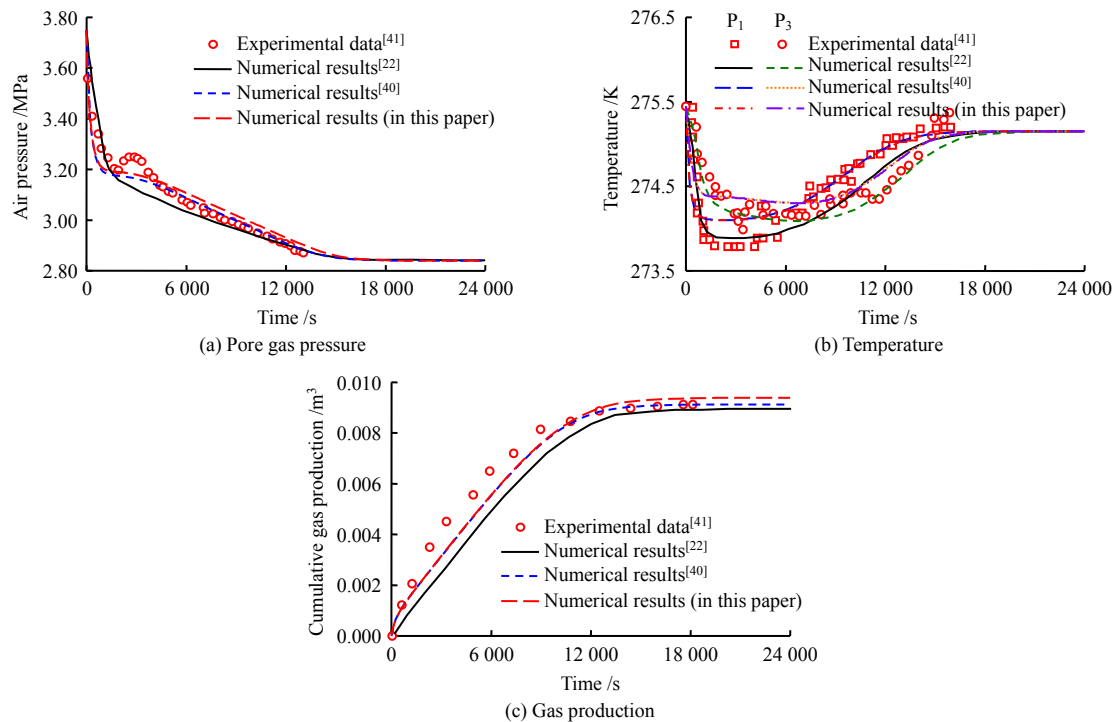


**Fig. 3 Comparisons of the evolution curves of physical parameters with time during hydrate decomposition**

3.2.2 Validation against large-scale numerical models for hydrate production

The model presented in this paper was used for calculation and comparison with the BP4-case2 of the model comparison<sup>[27]</sup>, which was initiated by the US Department of Energy and the National Energy Technology Laboratory, as shown in Fig. 4. The model was two-dimensional rotational axisymmetric with a radial length of 5 000 m. The initial state water pressure was 9.5 MPa, the total gas mole fraction was 0, and the temperature was 285.15 K. The distal boundary at a radius of 5 000 m was the same as the initial state; the water pressure at the production boundary was 3.1 MPa, and it was assumed that the heat flowed in and out freely through the temperature boundary with the fluid; the bulk modulus of the sediment was 22 GPa, the shear modulus was 22 GPa, and the pore water volumetric modulus was 2.16 GPa; the gas phase saturation at the initial moment was 0. The soil-water characteristic curve was modeled by the van Genuchten model, and the relative permeability of liquid and gas was modeled by the OPM model. The values of the modeling parameters are listed in Table 3, and the other parameters of the soil, water, gas and hydrate are shown in the literature<sup>[27]</sup>.

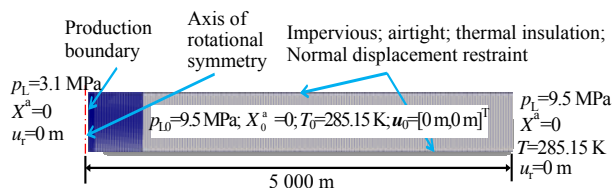


**Fig. 4 Mesh division and boundary conditions of the model**

Figure 5 shows the profiles of pore pressure, hydrate saturation and radial displacement at the 30th

day of hydrate production. Figure 5(a) shows the comparison of pore pressure obtained from this model and other software, which revealed that there were some differences between the numerical results of different software. This was caused by the differences in the coupling method of governing equations, the form of primary variable selection, the nonlinear and linear iteration methods, and the local equations of state adopted by different software, but the overall trend was the same. Figure 5(b) shows the hydrate saturation distribution profile, with a good consistency between the present model and most of the simulation results. It can be found that the variation of hydrate saturation was mainly concentrated in the range of 1-100 m in the radial direction, which corresponded to the large variation of pore pressure. Figure 5(c) shows the radial displacement profile, and the present model better captured the mechanical field response caused by hydrate decomposition. Therefore, the hydrate T-H-M model in this paper can effectively simulate the large-scale hydrate production process in the field.

3.3 Effect of pore water compressibility

This section investigates the effect of pore water compressibility on the coupled T-H-M response of sediments during the strong solid-liquid-gas phase transition of hydrate production. It also examines the numerical stability of NCP combined with the selection of special primary variables in dealing with the transition between single- and two-phase flows, which was analyzed using the previously mentioned large-scale model<sup>[27]</sup>. The pore water compressibility was characterized by the pore water bulk modulus, and four working conditions of 0.216, 2.160, 21.60 GPa, and infinity were taken to analyze the pore pressure, saturation and mechanical response at 30 d of the hydrate production.

**Table 3 Primary parameters of the model and their values<sup>[27]</sup>**

Model parameter	Expression	Value
SWRC	$p_c = \min \left( p_{C_{\max}}, p_0 \left( s_E \right)^{\frac{1}{n_{pc}}} - 1 \right)^{(1-n_{pc})}$ ; $s_E = \frac{s_L - s_{Lr}}{1 - s_{Lr}}$	$p_0 = 12.5 \text{ kPa}$ ; $p_{C_{\max}} = 5 \text{ MPa}$ ; $n_{pc} = 0.45$ ; $s_{Lr} = 0.11$
Relative permeability coefficient	$k_{\text{relL}} = \left( \frac{s_L - s_{Lr}}{1 - s_{Lr}} \right)^{n_L}$ ; $k_{\text{relG}} = \left( \frac{s_G - s_{Gr}}{1 - s_{Lr}} \right)^{n_G}$	$n_L = 3.0$ ; $n_G = 3.0$ ; $s_{Gr} = 0.02$ ; $s_{Lr} = 0.12$
Enthalpy change /( $\text{J} \cdot \text{mol}^{-1}$ )	$\Delta H = C_0 + C_1 T$	$C_0 = 55 \ 380.44$ ; $C_1 = -16.47$
Thermal conductivity coefficient /( $\text{W} \cdot \text{m}^{-1} \cdot \text{K}^{-1}$ )	$k_T = k_{T\text{dry}} + (\sqrt{s_L} + \sqrt{s_H})(k_{T\text{sat}} - k_{T\text{dry}})$	$k_{T\text{dry}} = 1.0$ ; $k_{T\text{sat}} = 3.1$

Note:  $p_{C_{\max}}$  is the maximum capillary suction;  $k_T$ ,  $k_{T\text{dry}}$ , and  $k_{T\text{sat}}$  are the thermal, saturated and dry thermal conductivity coefficients, respectively.

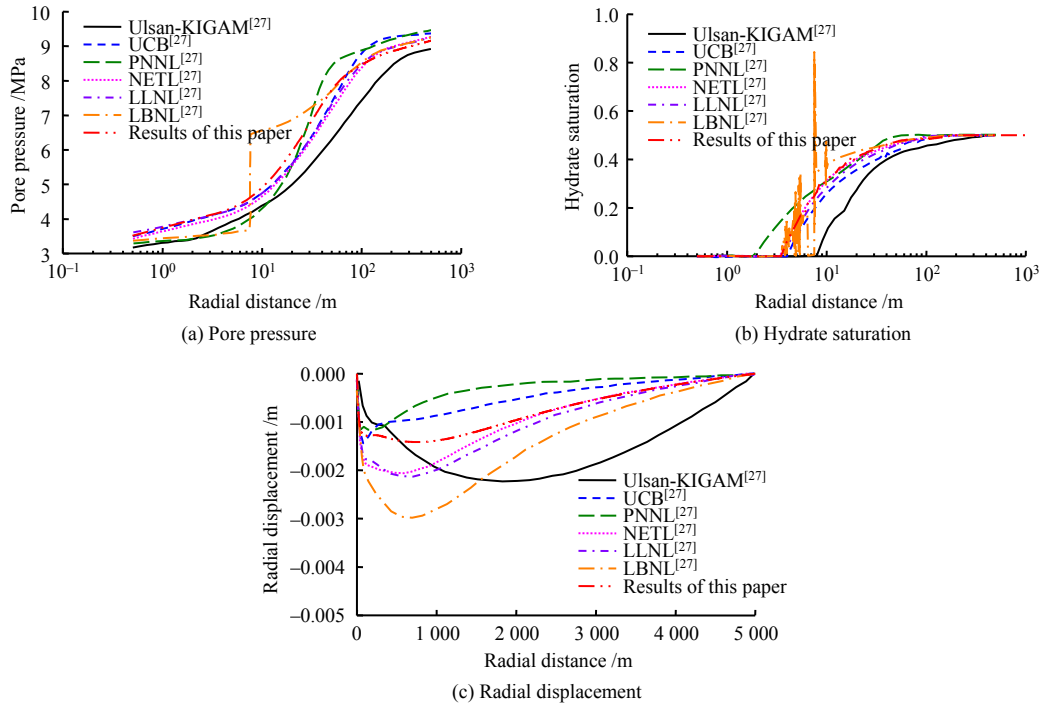


**Fig. 5 Comparisons of profile distribution at 30 d of hydrate production**

As shown in Fig. 6, the pore pressure profiles almost coincided within 100 m of the boundary of hydrate production using depressurization. However, there was a noticeable difference between 100 m and 1 000 m, which gradually disappeared in the range larger than 1 000 m. This was due to faster pore pressure dissipation and more pore water loss near the production boundary end, and the pore water expansion due to pressure drop was slower than the change of pore pressure dissipation, thus the pore pressure dissipation was dominant in this region. The pore pressure dissipation was of the same order of magnitude as the pore water expansion caused by pressure drop at the further end, and the pore pressure dissipation was slower when the pore water compressibility was considered. The pore water expansion caused by pressure drop was dominant further away, thus the pressure reached the distal boundary value at about 1 000 m when considering the pore water compressibility, i.e. the pressure influence range was smaller, while the pressure reached the boundary value only at the distal boundary when ignoring the pore water compressibility.

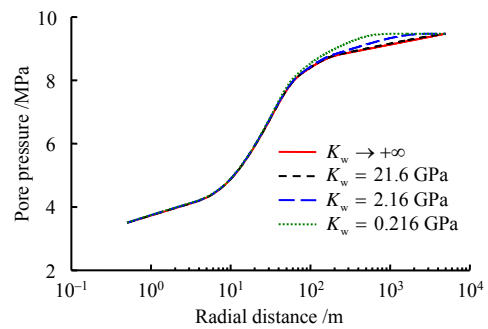


**Fig. 6 Effects of pore water compressibility on pore pressure**

Figure 7 shows the saturation distributions of gas phase, liquid phase and hydrate along the radial direction during hydrate decomposition. It can be found that the pore water compressibility did not have a significant effect on the saturation, and there was only a slight difference near 100 m, which was caused by the difference in pore pressure. The saturation varied from 30 m to 200 m. The gas saturation gradually increased from 0 to about 0.16 from the distal side to proximal side and maintained a constant

value near the production boundary. Moreover, the transition of gas phase saturation from 0 to non-zero verified the effectiveness of the NCP method combined with the selection of special primary variables in processing free transition problems between single- and two-phase flows. There was a small trough in the liquid phase saturation from the distal side to proximal side, and then it gradually increased to about 0.84, and remained constant near the production boundary. The hydrate saturation gradually decreased from the initial value of 0.5 to 0 from the distance of  $\sim 200$  m to  $\sim 30$  m; the closer the distance to the proximal side is, more drastic the change is. It is worth noting that the saturation of gas and liquid phases remained nearly constant for a certain distance at the production boundary and hardly changed at different moments, which is due to the fact that the hydrate has been completely decomposed in this zone, and the liquid and gas produced by the decomposition of the hydrate in the distal side reached a steady state of transport when arriving at this place. Since the viscosity of the gas phase was much smaller than that of the liquid phase, the gas phase saturation was lower than the liquid phase saturation at the steady state transport. This state was related to the gas production rate of the long-term hydrate exploitation, and the gas phase saturation of the steady transport state at the proximal exploitation side could be improved in practice by changing the permeability of the reservoir. It is interesting that the gas phase saturation gradually changed to non-zero starting from  $\sim 70$  m from far side to near side, while the liquid phase saturation gradually increased from  $\sim 200$  m from far side to near side (consistent with the distal position of hydrate saturation). Both of them showed spatial desynchronization, which was due to the fact that less gas was produced from hydrate decomposition at the initial stage, and all of it was dissolved in the liquid phase, thus the hydrate saturation decreased in the 70–200 m zone, the liquid phase saturation increased, and the gas phase saturation was maintained at zero. Subsequently, from about 70 m to the proximal side, the pore fluid was gradually transformed from the initial water-saturated single-phase state into the gas-liquid two-phase flow state, due to the decomposition of the hydrate to produce gas and liquid, the dissolution of the gas component to reach the maximum solubility and desolvation to release the free gas. This process was strongly nonlinear, which imposed high requirements on the stability and efficiency of numerical calculations. In the conventional non-isothermal two-phase flow theory, solving is generally performed using  $p_L / p_C$  and  $p_G$  as the primary variables for the water and gas mass conservation equation, in combination with the conventional liquid-gas two-phase state method. Additionally, the initial non-zero gas phase saturation needs to be artificially set to a very small value. However, describing the free gas precipitation and the resulting spatial distribution of liquid-gas saturation out of sync can be challenging. In addition, the

saturation degree easily exceeds the strict physical limit during the numerical iteration process, and the artificial forced constraints on the saturation degree range can easily cause the calculation results to be distorted or even non-convergence. In this paper, the model effectively described the process through the selection of special primary variables combined with the NCP method, as shown in the following. During the numerical computation process, the current dissolved gas was judged to reach the state of maximum solubility. If not reached, then there was only a non-zero liquid phase saturation, and if reached, then there were non-zero liquid phase and gas phase saturations at the same time. Since the NCP was established by considering two states at the same time, the two cases were finally solved by the NCP constraint equations without artificial constraints, and the numerical iterative solving process was stable. In combination with the adaptive time-step method, the time step of numerical computation can be greatly increased. For example, the initial time step of this model was 1 s, and the maximum time step in the later stage was up to 10 000 s, which resulted in a highly efficient numerical solution.

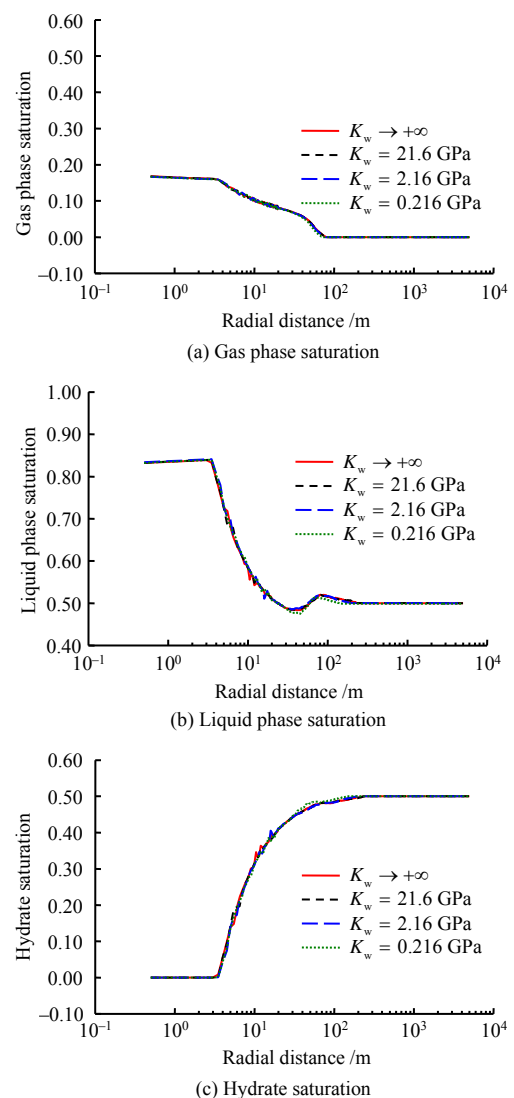
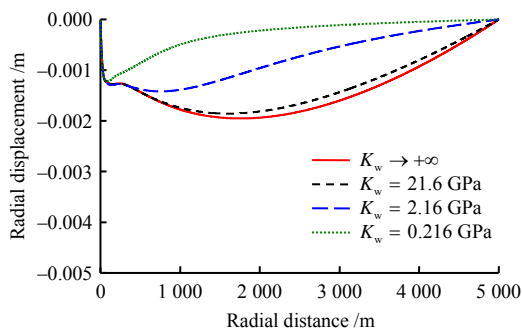


Fig. 7 Effects of pore water compressibility on saturation

Figure 8 shows the distribution of radial displacements from hydrate decomposition to the 30th day. It can be observed that the displacements showed obvious differences in varying pore water compressibility. When the pore water compressibility was ignored, the displacement first increased from the proximal side to distal side, and then continued to change in a wide range, with the peak occurring at about 2 000 m. With the increase in pore water compressibility, the peak gradually shifted forward, and the closest point to the production well was at about 100 m. This is due to the fact that when the pore water compressibility is not considered, the pressure is instantaneously transferred to the distal side, which has a large influence on the deformation range. When the pore water compressibility is considered, the small pressure drop at the distal side is supplemented by the pore water expansion caused by pressure drop, and its influence is within a certain region. In the large-scale validation algorithm of Section 3.2.2<sup>[27]</sup>, the radial displacement distribution curves obtained by Ulsan-KIGAM<sup>[27]</sup> displayed the former characteristics, while the curves given by UCB et al.<sup>[27]</sup> showed the latter characteristics. Since the deformation of hydrate deposits affects the stability of the reservoir during production, the degree of deformation is not negligible at high pore pressures even though ignoring pore water compressibility overestimates its degree of deformation.



**Fig. 8** Effects of pore water compressibility on radial displacement

## 4 Conclusions

To address the multiphase multi-field coupling problem in the hydrate production process, a coupled analytical model of T-H-M for hydrate production was developed based on the open-source finite element platform OpenGeoSys. The model considered the equations of water and gas mass conservation, energy conservation, conservation of linear momentum and pore water compressibility in the solid-liquid-gas phase transition during hydrate decomposition. The pore water pressure, total gas phase mole fraction, temperature and displacement were selected as the primary variables, and combined with the selection of special primary variables, the locally embedded NCP method strictly constrained the range of liquid-gas saturation. The main conclusions are drawn as follows:

(1) This model was verified by comparing it with

the laboratory decomposition test and the large-scale numerical model of hydrate production using depressurization, and the effectiveness of combination of local NCP and the selection of special primary variables to solve the problem was verified by simulating the process of gas phase generation. The model was developed based on the open-source software and was numerically stable and efficient in addressing strongly nonlinear problems such as solid-liquid-gas phase transitions and pore-fluid phase generation/disappearance.

(2) The pore water compressibility during the large pore pressure change in the process of hydrate production using depressurization needs to be considered. The pore water expansion caused by pressure drop during the hydrate production using depressurization compensated for the pore pressure drop at the distal side to a certain extent, and the neglect of the pore water compressibility will lead to the overestimation of the change of pressure at the distal side and the amount of deformation of the sediment caused by it, which is unfavorable to the economy and safety of the design of the production facilities.

(3) Hydrate gradually decomposed from proximal side to distal side in the process of hydrate production using depressurization, and the development of gas phase saturation lagged behind that of liquid phase saturation due to the influence of gas phase dissolution in the initial saturation state. The generated gas and liquid gradually moved towards the production boundary and reached a stable transport state, and the saturation of gas and liquid phases tended to stabilize during the stable liquid-gas transport. Since the viscosity of the gas phase was much lower than that of the liquid phase, the gas phase saturation was lower than the liquid phase saturation, which could be used to assess the gas production rate during the stabilized production, and provide a basis for evaluating and upgrading the efficiency of the actual hydrate production.

## References

- [1] SLOAN E D, KOH C A. Clathrate hydrates of natural gases[D]. Boca Raton: CRC Press, 2008.
- [2] KVENVOLDEN K A. Methane hydrate—a major reservoir of carbon in the shallow geosphere[J]. *Chemical Geology*, 1988, 71(1-3): 41–51.
- [3] MILKOV A V. Global estimates of hydrate-bound gas in marine sediments: how much is really out there[J]. *Earth-Science Reviews*, 2004, 66(3–4): 183–197.
- [4] YUAN Si-min, WANG Lu-jun, ZHU Bin, et al. Volumetric strain analysis model for gas hydrate-bearing sediment considering effects of hydrate dissociation[J]. *Chinese Journal of Geotechnical Engineering*, 2022, 44(6): 1044–1052.
- [5] YAN Rong-tao, WEI Chang-fu, WEI Zhen-hou, et al. Effect of hydrate formation on mechanical strength of hydrate-bearing sand[J]. *Chinese Journal of Geotechnical Engineering*, 2012, 34(7): 1234–1240.
- [6] LIANG Wen-peng, ZHOU Jia-zuo, CHEN Pan, et al. An elastoplastic constitutive model of gas hydrate bearing sediments based on homogenization theory[J]. *Rock and Soil Mechanics*, 2021, 42(2): 481–490.
- [7] LIU Yan-jing, WANG Lu-jun, ZHU Bin, et al. An elastoplastic constitutive model for hydrate-bearing sediments considering the effects of filling and bonding[J].

- Rock and Soil Mechanics, 2022, 43(9): 2471–2482.
- [8] MCCONNELL D R, ZHANG Z, BOSWELL R. Review of progress in evaluating gas hydrate drilling hazards[J]. *Marine and Petroleum Geology*, 2012, 34(1): 209–223.
- [9] XU Bin, ZOU De-gao, ZHOU Dan, et al. Analysis method on stability of the submarine slope due to methane hydrate dissociation[J]. *China Civil Engineering Journal*, 2011, 44(Suppl.2): 207–211.
- [10] JIANG Ming-jing, XIAO Yu, LIU Fang. Methodology for assessing seabed instability induced by exploitation of methane hydrate[J]. *Chinese Journal of Geotechnical Engineering*, 2010, 32(9): 1412–1417.
- [11] MAKOGON Y F, HOLDITCH S A, MAKOGON T Y. Natural gas-hydrates-a potential energy source for the 21st Century[J]. *Journal of Petroleum Science and Engineering*, 2007, 56(1–3): 14–31.
- [12] YAMAMOTO K, DALLIMORE S. Aurora-JOGMEC-NRCan Mallik 2006–2008 gas hydrate research project progress[J]. *Fire in the Ice*, 2008, 7(2): 1–5.
- [13] BOSWELL R, SCHODERBEK D, COLLETT T S, et al. The Ignik Sikumi field experiment, Alaska North Slope: design, operations, and implications for CO<sub>2</sub>-CH<sub>4</sub> exchange in gas hydrate reservoirs[J]. *Energy and Fuels*, 2017, 31(1): 140–153.
- [14] KONNO Y, FUJII T, SATO A, et al. Key findings of the world's first offshore methane hydrate production test off the coast of Japan: toward future commercial production[J]. *Energy and Fuels*, 2017, 31(3): 2607–2616.
- [15] YU T, GUAN G, ABUDULA A. Production performance and numerical investigation of the 2017 offshore methane hydrate production test in the Nankai Trough of Japan[J]. *Applied Energy*, 2019, 251: 113338.
- [16] LI J F, YE J L, QIN X W, et al. The first offshore natural gas hydrate production test in South China Sea[J]. *China Geology*, 2018, 1(1): 5–16.
- [17] YE J L, QIN X W, XIE W W, et al. The second natural gas hydrate production test in the South China Sea[J]. *China Geology*, 2020, 3(2): 197–209.
- [18] SLOAN E D. Fundamental principles and applications of natural gas hydrates[J]. *Nature*, 2003, 426(6964): 353–359.
- [19] CHEN X, LU H, GU L, et al. Preliminary evaluation of the economic potential of the technologies for gas hydrate exploitation[J]. *Energy*, 2022, 243: 123007.
- [20] RUTQVIST J, MORIDIS G J, GROVER T, et al. Geomechanical response of permafrost-associated hydrate deposits to depressurization-induced gas production[J]. *Journal of Petroleum Science and Engineering*, 2009, 67(1–2): 1–12.
- [21] JIN G, LEI H, XU T, et al. Simulated geomechanical responses to marine methane hydrate recovery using horizontal wells in the Shenhu area, South China Sea[J]. *Marine and Petroleum Geology*, 2018, 92: 424–436.
- [22] SUN X, LI Y, LIU Y, et al. The effects of compressibility of natural gas hydrate-bearing sediments on gas production using depressurization[J]. *Energy*, 2019, 185: 837–846.
- [23] ZHANG Xiao-ling, XIA Fei, DU Xiu-li, et al. Study on multi-field coupling model considering damage of hydrate-bearing sediments[J]. *Rock and Soil Mechanics*, 2019, 40(11): 4229–4239, 4305.
- [24] SÁNCHEZ M, SANTAMARINA C, TEYMOURI M, et al. Coupled numerical modeling of gas hydrate-bearing sediments: from laboratory to field-scale analyses[J]. *Journal of Geophysical Research: Solid Earth*, 2018, 123(12): 10326–10348.
- [25] WAN Y, WU N, CHEN Q, et al. Coupled thermal-hydrodynamic-mechanical-chemical numerical simulation for gas production from hydrate-bearing sediments based on hybrid finite volume and finite element method[J]. *Computers and Geotechnics*, 2022, 145: 104692.
- [26] WILDER J W, MORIDIS G J, WILSON S J, et al. An international effort to compare gas hydrate reservoir simulators[C]//Proceedings of 6th International Conference on Gas Hydrates (ICGH 2008). Vancouver: [s. n.], 2008.
- [27] WHITE M D, KNEAFSEY T J, SEOL Y, et al. An international code comparison study on coupled thermal, hydrologic and geomechanical processes of natural gas hydrate-bearing sediments[J]. *Marine and Petroleum Geology*, 2020, 120: 104566.
- [28] LI B, LIANG Y P, LI X S, et al. A pilot-scale study of gas production from hydrate deposits with two-spot horizontal well system[J]. *Applied Energy*, 2016, 176: 12–21.
- [29] WANG Lu-jun, WANG Peng, ZHU Bin, et al. Development and application of centrifuge in-flight apparatus for hydrate exploitation modelling[J/OL]. *Chinese Journal of Geotechnical Engineering*, 2023, <http://kns.cnki.net/kcms/detail/32.1124.TU.20230305.2212.036.html>.
- [30] WANG Xin-bo, WANG Lu-jun, ZHU Bin, et al. Experimental study of behavior of hydrate-bearing sediments during servo depressurization[J]. *Rock and Soil Mechanics*, 2022, 43(9): 2360–2370.
- [31] COATS K H. An equation of state compositional model[J]. *Society of Petroleum Engineers Journal*, 1980, 20(5): 363–376.
- [32] CLASS H, HELMIG R, BASTIAN P. Numerical simulation of non-isothermal multiphase multicomponent processes in porous media: 1. an efficient solution technique[J]. *Advances in Water Resources*, 2002, 25(5): 533–550.
- [33] FIROOZABADI A. *Thermodynamics of hydrocarbon reservoirs*[M]. New York: McGraw-Hill, 1999.
- [34] MOORTGAT J, LI Z, FIROOZABADI A. Three-phase compositional modeling of CO<sub>2</sub> injection by higher-order finite element methods with CPA equation of state[J]. *Water Resources Research*, 2012, 48: 12511.
- [35] BOURGEAT A, JURAK M, SMAĚ F. Two-phase, partially miscible flow and transport modeling in porous media; application to gas migration in a nuclear waste repository[J]. *Computational Geosciences*, 2009, 13: 29–42.
- [36] ABADPOUR A, PANFILOV M. Method of negative saturations for modeling two-phase compositional flow with oversaturated zones[J]. *Transport in Porous Media*, 2009, 79(2): 197–214.
- [37] NEUMANN R, BASTIAN P, IPPISCH O. Modeling and simulation of two-phase two-component flow with disappearing nonwetting phase[J]. *Computational Geosciences*, 2013, 17: 139–149.
- [38] LAUSER A, HAGER C, HELMIG R, et al. A new approach for phase transitions in miscible multi-phase flow in porous media[J]. *Advances in Water Resources*, 2011, 34(8): 957–966.
- [39] HAGER C, WOHLMUTH B I. Semismooth Newton methods for variational problems with inequality constraints[J]. *GAMM-Mitteilungen*, 2010, 33(1): 8–24.
- [40] YE Z G, WANG L J, ZHU B, et al. A thermo-hydro-chemo-mechanical coupled model for natural gas hydrate bearing sediments considering gravity effect[J]. *Journal of Natural Gas Science and Engineering*, 2022, 108: 104823.
- [41] MASUDA Y, FUJINAGA Y, NAGANAW S, et al. Modeling and experimental studies on dissociation of methane gas hydrates in Berea sandstone cores[C]//Proceedings of the third International Gas Hydrate Conference. Salt Lake City, USA: [s. n.], 1999.
- [42] DENG X, FENG J, PAN S, et al. An improved model for the migration of fluids caused by hydrate dissociation in porous media[J]. *Journal of Petroleum Science and Engineering*, 2020, 188: 106876.